Published online 23 June 2021

Nucleic Acids Research, 2021, Vol. 49, No. 12 ***6941–6957***
https://doi.org/10.1093/nar/gkab512

Formation of frameshift-stimulating RNA pseudoknots is facilitated by remodeling of their folding intermediates

Chiung-Fang Hsu[1,†], Kai-Chun Chang[1,†], Yi-Lan Chen[2], Po-Szu Hsieh[1], An-I Lee[1], Jui-Yun Tu[1], Yu-Ting Chen[1] and Jin-Der Wen[1,2,*]

[1]Institute of Molecular and Cellular Biology, National Taiwan University, Taipei 10617, Taiwan and [2]Genome and Systems Biology Degree Program, National Taiwan University and Academia Sinica, Taipei 10617, Taiwan

Received November 11, 2020; Revised May 27, 2021; Editorial Decision May 31, 2021; Accepted June 04, 2021

ABSTRACT

Programmed –1 ribosomal frameshifting is an essential regulation mechanism of translation in viruses and bacteria. It is stimulated by mRNA structures inside the coding region. As the structure is unfolded repeatedly by consecutive translating ribosomes, whether it can refold properly each time is important in performing its function. By using single-molecule approaches and molecular dynamics simulations, we found that a frameshift-stimulating RNA pseudoknot folds sequentially through its upstream stem S1 and downstream stem S2. In this pathway, S2 folds from the downstream side and tends to be trapped in intermediates. By masking the last few nucleotides to mimic their gradual emergence from translating ribosomes, S2 can be directed to fold from the upstream region. The results show that the intermediates are greatly suppressed, suggesting that mRNA refolding may be modulated by ribosomes. Moreover, masking the first few nucleotides of S1 favors the folding from S2 and yields native pseudoknots, which are stable enough to retrieve the masked nucleotides. We hypothesize that translating ribosomes can remodel an intermediate mRNA structure into a stable conformation, which may in turn stimulate backward slippage of the ribosome. This supports an interactive model of ribosomal frameshifting and gives an insightful account addressing previous experimental observations.

INTRODUCTION

RNA's function is manifested in its sequences and structures. A nucleotide sequence may form alternative structures that perform distinct functions (1), like riboswitches (2) and ribozymes (3). Nascent RNA will start to fold when a sufficient length has emerged from the RNA polymerase. Such co-transcriptional folding (4) is affected by the availability of downstream sequences (5,6), as well as the presence of ligands (7). Thus, other structures besides the native conformations can form. These mis-folded structures generally result from kinetically trapped intermediates in a rugged folding energy landscape and can be rescued by RNA chaperones (1,8–12).

Messenger RNA (mRNA) provides a single-stranded template as the reading frame for protein synthesis. Structures formed inside the coding region are disrupted repetitively by consecutive translating ribosomes and refold after each of the ribosomes passes. This ribosome-mediated refolding process is similar to the co-transcriptional folding. Thus, depending on the translational rate and ribosomal pausing, the ribosome-mediated mRNA refolding may result in alternative structures, which the successive ribosomes will encounter and be affected differently. This is particularly critical in some biological processes, such as programmed –1 ribosomal frameshifting (–1 PRF), which is stimulated by mRNA structures.

In many viruses and bacteria, –1 PRF is employed to regulate the relative expression level of two proteins encoded in the same mRNA (13–17). Two elements of mRNA are required to facilitate –1 PRF: a heptanucleotide slippery sequence and a structure (e.g. a stem-loop or a pseudoknot) located 5–9 nucleotides downstream from the slippery sequence (14). The structure can stimulate the ribosome to slip backward while it is translating the slippery sequence. Characteristics of the structure, such as thermal sta-

*To whom correspondence should be addressed. Tel: +886 2 33662486; Fax: +886 2 33662478; Email: jdwen@ntu.edu.tw
†The authors wish it to be known that, in their opinion, the first two authors should be regarded as Joint First Authors.
Present address: Kai-Chun Chang, Department of Bioengineering and Therapeutic Sciences, Schools of Medicine and Pharmacy, University of California, San Francisco, CA 94158, USA.

bility (18–20), mechanical stability (21,22), and conformational plasticity (23–31) influence frameshifting, but controversy remains as to which characteristic is the most influential. During frameshifting, tension is supposed to be built along the mRNA between the structure and the tRNA-binding sites of the ribosome (32–35), so it may be expected that the mechanical strength of the structure plays a key role. Interestingly, by using optical tweezers to measure the mechanical and folding properties of a variety of viral frameshift-stimulating pseudoknots, Ritchie *et al.* found that frameshifting efficiency was correlated mostly with the propensity of the pseudoknot to fold into alternative structures (termed conformational plasticity) and not with its structural stability (23). More insights into the conformational plasticity were revealed recently for the frameshifting stimulator of the West Nile virus (WNV) (30), which could yield –1 PRF with an efficiency of up to 70–80% (27). The WNV frameshifting stimulator was reported to form diverse interchangeable conformations through different folding pathways in a force range of 7–13 pN (30); this range is just below the force (∼13 pN) that has been shown to stall actively translating ribosomes (36). How such RNA conformational interchanges can lead to ribosomal frameshifting remains unclear, but the force that interacts between the ribosome and the RNA structures appears to be involved.

Accordingly, the capability of forming a stable and unwinding-resistant conformation to impede translating ribosomes may remain indispensable for efficient frameshifting stimulators. For example, compared to non-frameshifted ribosomes, the ribosomes that shifted into the –1 frame were shown to pause, with a tenfold longer dwell time, upon encountering a G/C-rich stem-loop structure (37). Another example is the DU177 pseudoknot, which is derived from the human telomerase RNA and stabilized by three major groove and two minor groove base triples (see Figure 1) (38). When this pseudoknot is used as a frameshifting stimulator (22,39,40), its various structural components can be changed to fine-tune the structural stability to delineate how the stability affects frameshifting efficiency. As demonstrated by Chen et al., DU177 and its mutants (frameshifting efficiencies: 0–53%) preferred forming intermediate (alternative) structures, but only those with higher unfolding forces (≥45 pN) can result in higher frameshifting efficiencies (>20%) (22). However, whether frameshifting stimulators can indeed tolerate ribosomal unwinding during translation, and how this may occur, has not been demonstrated. In addition, as the frameshifting stimulator of mRNA is subjected to multiple unfolding-refolding cycles by consecutive translating ribosomes, whether the ribosome-mediated RNA refolding preserves a similar tendency as the full-length sequence folds to form alternative structures is not clear.

In this study, we used optical tweezers (41,42) to measure the unfolding and refolding transitions of the DU177 pseudoknot. We demonstrate that the dominant folding pathway followed the sequential formation of stems S1 and S2 and resulted in a low population (<20%) of native pseudoknot conformations. Interestingly, when the last two nucleotides (nt) of the pseudoknot were masked by a complementary DNA strand, the formation efficiency of native structures was greatly increased to almost 90%. The aim of this approach (masking the last 2 nt of the structure) was to mimic the refolding of mRNA when it has not yet completely emerged from the exit site of the ribosome that has just unfolded and passed through the structure. Thus, the results suggest that an mRNA pseudoknot can have a higher probability of refolding into its native conformation during translation than when measured with a bare sequence. On the other hand, when the first 2 nt of stem S1 were masked in a similar way, the folding pathway was opposite: stem S2 formed first, followed by stem S1. Surprisingly, all detected structures were in the native conformation (∼100%), and the two masked nucleotides were retrieved so that the full length of stem S1 was restored. The stem S2-first folding pathway appeared to bypass any stable intermediates and to strengthen the terminal end of stem S1, as previously demonstrated (40). Indeed, we found that stem S1 of the DU177 pseudoknot was resistant to unwinding by the ribosome stalled at the position corresponding to the slippery sequence. These results support the hypothesis that a frameshifting stimulator, during its refolding into a more stable conformation, can compete with the ribosome for the ribosome-occupied nucleotides and potentially cause backward slippage of the ribosome. Our study provides unforeseen insights into the mechanism of mRNA pseudoknot remodeling in stimulating ribosomal frameshifting.

MATERIALS AND METHODS

Preparation of RNA constructs for optical tweezers experiments

RNA constructs used for optical tweezers experiments were prepared as previously described (40). DNA oligomers corresponding to DU177 and other related RNA sequences were chemically synthesized and cloned into pVE60hp (43) between NdeI and BsrGI sites. The resultant plasmid was cut at the BssSI site (∼900 bp downstream of the cloning site) and transcribed *in vitro* from the T7 promoter (∼750 bp upstream of the cloning site) to the cleaved site using MEGAscript T7 Transcription Kit (Invitrogen). To facilitate measurements of structure-forming RNA with the optical tweezers, two complementary DNA handles were respectively prepared using PCR, tag-labeled [with a digoxigenin tag on the upstream handle (737 bp) and a biotin tag on the downstream handle (917 bp)], and then annealed to the flanking regions of the structure (44).

Measurements using optical tweezers

To measure folding-unfolding transitions of RNA structures, the digoxigenin and biotin tags at the two ends of the RNA construct were immobilized on two polystyrene beads (2.1 μm in diameter; Spherotech) coated with anti-digoxigenin antibody and streptavidin, respectively. One bead was fixed on the tip of a micropipette and the other was held by a dual-beam force-measuring optical trap (45). Two types of force manipulation protocols (force-ramping and force-drop) were applied to the tethered RNA molecule. For force-ramping experiments, the distance between beads was increased by moving the trap in a speed of 100 nm/s, such that the force imposed on RNA was gradually raised

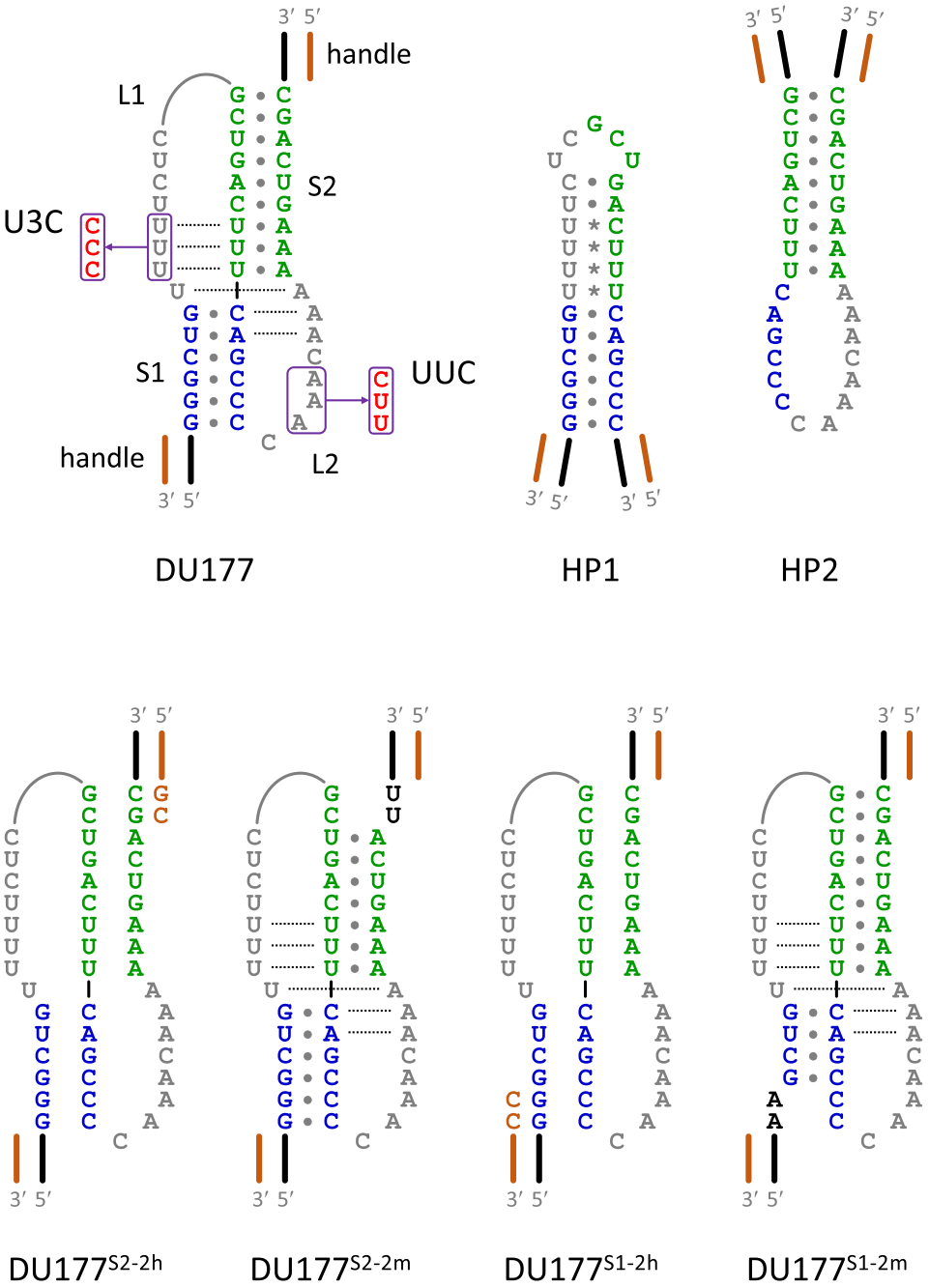

Figure 1. Schematics of DU177-related RNA structures. Stem S1 of the pseudoknot is shown in blue, S2 in green, and loops L1 and L2 in gray. Watson-Crick and non-Watson-Crick base pairs are denoted by filled circles and asterisks, respectively. Base triples and the Hoogsteen base pair in DU177 are connected by dotted lines. U3C and UUC are mutants with base substitutions in loops L1 and L2, respectively. $DU177^{S2\text{-}2m}$ and $DU177^{S1\text{-}2m}$ are mutants with 2-bp disruption in stems S2 and S1, respectively. DNA handles (not to scale) annealed to the flanking regions are shown in brown. Sequences extended from the handles that are complementary to the last two nucleotides in stem S2 ($DU177^{S2\text{-}2h}$) or the first two nucleotides in stem S1 ($DU177^{S1\text{-}2h}$) are shown. The base-pairing states in $DU177^{S2\text{-}2h}$ and $DU177^{S1\text{-}2h}$ are not denoted. HP1 and HP2, isolated hairpins of stem S1-loop L1 and stem S2-loop L2 of DU177, respectively.

to unfold the structures. Upon reaching the preset maximum value (depending on the construct measured; for example, 45 pN for DU177), the force was decreased in the same speed to 2 pN by inversing the direction of the trap movement to let RNA refold. When indicated, 10 s of extra incubation time was allowed for RNA refolding at the minimum force (2 pN). This unfolding-refolding procedure was repeated. The force-drop experiments followed a similar protocol, except that the force was quickly dropped from the highest value and maintained at a moderate tension (e.g. 10 pN). At the constant force, the folding progress of RNA could be followed by its extension (end-to-end distance) change in real time (46,47). The measurements were done in 10 mM Tris–HCl, pH 7.0, 200 mM NaCl, and 0.1 mM EDTA. To ensure that the measurements were from single tethers, we routinely increased the force up to 60–70 pN at the end of experiments; a single tether would break in one single step or showed overstretching of the RNA/DNA handles (48) at ∼55 pN in the buffer mentioned above.

Data from optical tweezers were acquired at 1000 Hz and averaged to 100 Hz for further analysis using custom-written MATLAB (MathWorks) programs. An extensible worm-like chain (WLC) model (49,50) was used to predict the extension change (Δx) of a specified RNA structure unfolded at a given force (F):

$$F = \frac{k_B T}{P}\left[\frac{1}{4(1-\Delta x/L+F/K)^2} - \frac{1}{4} + \frac{\Delta x}{L} - \frac{F}{K}\right]$$

where k_B is Boltzmann's constant, P is the persistent length, T is the absolute temperature, L is the contour length, and K is the stretch modulus. For single-stranded RNA, the values of P, L and K are 1 nm, 0.59 nm/nucleotide, and 1500 pN, respectively (51,52). The finite distance between the termini of the folded structure has to be subtracted from the calculated Δx to reflect the expected extension change when measured by optical tweezers. This distance is 2 nm for a stem-loop structure and 4.8 nm for the fully-folded DU177 pseudoknot (PDB ID: 2K96).

Construction of fluorescent dye-labeled mRNA

FRET dye-pair-labeled mRNA was prepared by ligation of three RNA oligomers: rbs, Cy3-labeled rna1, and Cy5-labeled rna2. The rbs strand was chemically synthesized (GE Dharmacon) or transcribed *in vitro* with the hepatitis delta virus (HDV) ribozyme fused at the 3′ end, where self-cleavage of the HDV ribozyme at its 5′ end would produce a homogeneous 3′ end of rbs (53). After transcription, five thermal cycles (70°C for 10 s, 50°C for 1 min, and 37°C for 10 min) (54) were performed to promote folding and self-cleavage of the ribozyme. The products were resolved on denaturing polyacrylamide gel electrophoresis (containing 7.6 M urea) and the rbs strand was excised and purified using ZR small-RNA PAGE Recovery Kit (Zymo Research).

The rna1and rna2 strands were synthesized by GE Dharmacon; the base for dye labeling was replaced with 5-aminoallyl-uridine (5NU). Note that there were three variants of rna1 (rna1_DU177, rna1_U3C and rna1_HP2), specific for the constructs of DU177, U3C, and HP2, respectively. The RNA oligomers were reacted with at least a 3-fold molar excess of Cy3-NHS (for rna1) or Cy5-NHS (for rna2) (Lumiprobe) in 25 mM $NaHCO_3$ at room temperature overnight. The reaction was quenched with NH_2OH-HCl (to a final concentration of 0.8 M) at room temperature for 15 min and then ethanol-precipitated. The dye-labeled strands were purified using a C8 reversed phase HPLC column (PerkinElmer).

Full-length mRNA was made by DNA-splinted RNA ligation (55). The three RNA strands (rbs, Cy3-labeled rna1, and Cy5-labeled rna2) were annealed with the corresponding splint DNA by heating at 75°C for 5 min and then cooling to 20°C at −1°C/min. They were then ligated with T4 DNA ligase (New England Biolabs) at 25°C overnight. The splint DNA was digested by RNase-free TURBO DNase (Ambion). Finally, the full-length, FRET dye-labeled mRNA was purified by denaturing polyacrylamide gel electrophoresis.

Sequences of RNA oligomers are shown below (in 5′ to 3′):

rbs:UAGGAGGUAUAAUAUGUUUAAAGAG
rna1_DU177: UACGGGCUGUUUUUC(5NU)CGCU GACUUUCAG
rna1_U3C: UACGGGCUGUCCCUC(5NU)CGCUGA CUUUCAG
rna1_HP2: CCC(5NU)CGCUGACUUUCAG
rna2: CCC(5NU)AAACAAAAAAGUCAGCA

Sequences of splint DNA are shown below (in 5′ to 3′):

splint_DU177:TGCTGACTTTTTTGTTTAGGGCTG AAAGTCAGCGAGAAAAACAGCCCGTACTCTTT AAACATATTATACCTCCTA
splint_U3C:TGCTGACTTTTTTGTTTAGGGCTGAA AGTCAGCGAGAGGGACAGCCCGTACTCTTTAA ACATATTATACCTCCTA
splint_HP2:TGCTGACTTTTTTGTTTAGGGCTGAA AGTCAGCGAGGGCTCTTTAAACATATTATACCT CCTA

Purification of biotinylated ribosomes

The biotinylated 70S ribosomes were purified from *Escherichia coli* strain KLF203 (36) (originally obtained from Harry Noller, University of California, Santa Cruz), in which the C terminal of the ribosomal protein bS16 was fused with the biotinylation domain of the biotin carboxyl carrier protein (BCCP). Biotinylation of the fusion protein was highly efficient *in vivo* (36).

Typically, bacteria were grown at 37°C in 2.4 l of LB (Luria-Bertani) broth to ∼0.6 OD_{600}, pelleted, and stored at −80°C. The frozen cells were resuspended in a 7-fold volume of Buffer A [20 mM Tris–HCl, pH 7.2, 100 mM NH_4Cl, 10 mM $MgCl_2$, 6 mM β-mercaptoethanol (β-ME), and 0.5 mM EDTA] and lysed by three passes through a French press (Constant Systems, CF Range) at 20 Kpsi. The lysate was cleared by centrifugation and layered onto 37.7% sucrose cushions made in Buffer B (20 mM Tris–HCl, pH 7.2, 500 mM NH_4Cl, 10 mM $MgCl_2$, 6 mM β-ME and 0.5 mM EDTA). Centrifugation was done in a P40ST rotor (Hitachi) at 33,800 rpm for 18 h at 4°C. The ribosome pellets were resuspended in Buffer C [20 mM Tris-OAc, pH 7.5, 60 mM NH_4Cl, 7.5 mM $Mg(OAc)_2$, 6 mM β-ME and 0.5 mM

EDTA], layered onto 10–40% sucrose gradients made in Buffer C, and centrifuged in a P28S rotor (Hitachi) at 15,800 rpm for 17 h at 4°C. The fractions corresponding to the 70S ribosomes were collected and dialyzed against Buffer C at 4°C overnight. Finally, the samples were aliquoted, flash-frozen in liquid nitrogen, and stored at −80°C.

Purification of initiation and elongation factors

The EF-Tu gene was cloned from *E. coli* strain MRE600 and inserted into pET24b(+) between NdeI and XhoI with a His6 tag at the C terminal. BL21-CodonPlus (DE3)-RIPL competent cells (Agilent) were transformed with the plasmid and grown at 37°C in 1 l of LB broth containing 50 μg/ml kanamycin to ∼0.6 OD_{600}. Isopropyl β-D-1-thiogalactopyranoside (IPTG) was added to a final concentration of 1 mM to induce EF-Tu production. Cells continued to grow for 2 h, were then collected, resuspended in Binding Buffer (50 mM Tris–HCl, pH 7.5, 60 mM NH_4Cl, 7 mM $MgCl_2$, 20 mM imidazole, 15% glycerol, 10 μM GDP and 6 mM β-ME), and disrupted by three passes through the French press at 20 Kpsi. The lysate was cleared by centrifugation and loaded onto a HisTrap FF crude column (5 ml, GE Healthcare). The column was washed with 25 ml of Binding Buffer plus 500 mM KCl and then eluted by 50 ml of a linear gradient of imidazole (20–250 mM). The protein (appeared at a peak of ∼120 mM imidazole) was collected, concentrated, and dialyzed against Storage Buffer (50 mM Tris–HCl, pH 7.5, 60 mM NH_4Cl, 7 mM $MgCl_2$, 15% glycerol, 20 μM GDP and 6 mM β-ME). Finally, the samples were aliquoted, flash-frozen in liquid nitrogen, and stored at −80°C.

The plasmids containing the IF2, IF3 and EF-G genes were originally obtained from the Noller lab and had a design similar to EF-Tu. The His6 tag of IF1 was fused to the N terminal instead. These proteins were produced and purified similarly to the EF-Tu method described above.

Preparation of initiation complexes and stalled elongation complexes

The initiation complex (IC) was formed by incubating 0.2–1 μM FRET dye-pair-labeled mRNA, 1–5 μM biotinylated 70S ribosomes, 1 μM fMet-$tRNA^{fMet}$, 1.25 μM each of the initiation factors (IF1, IF2 and IF3), and 1 mM GTP in TLB buffer [40 mM HEPES–KOH, pH 7.5, 70 mM NH_4Cl, 7 mM $Mg(OAc)_2$ and 3.7 mM β-ME] at 37°C for 15 min. The sample was diluted, injected into a glass chamber, and immobilized on the NeutrAvidin-coated surface through the biotinylated ribosomes. To stall the ribosomes at indicated codons, a translation mixture (TM) was prepared in TLB buffer containing 1.4 μM EF-Tu, 0.14 μM EF-G, 1 mM GTP, and 0.14–0.28 μM each of the specified aminoacyl-tRNAs (including $tRNA^{Phe}$, $tRNA^{Lys}$ and $tRNA^{Glu}$; Sigma). The TM was mixed with 5 volumes of oxygen scavenging solution [OSS; 1.7 mM Trolox, 2.6 mM protocatechuic acid (PCA, Sigma-Aldrich) and 0.21 U/ml protocatechuate 3,4-dioxygenase (PCD, OYC Americas) in TLB buffer] and injected into the chamber. The chamber was heated at 37°C on a hot plate for 15 min and then moved to the microscope for FRET recording at room temperature.

Single-molecule FRET measurements

Single-molecule FRET experiments were carried out on a home-built objective-type total internal reflection fluorescence (TIRF) microscope as described previously (40). In addition to the green laser, we added a red laser (638 nm, 35 mW, DL638-035, CrystaLaser) to the microscope to identify and exclude Cy5-bleached or Cy3-only molecules. Movies were recorded by the SMET package (56) at 20 Hz and processed by IDL scripts (https://cplc.illinois.edu/software/) (57). Time-evolved smFRET data were analyzed by custom-written MATLAB programs.

Molecular dynamics (MD) simulations

The MD simulations protocol was slightly modified from our previous report (35). Briefly, each simulation system was prepared and solvated in TIP3P water using tLeap from AMBER18 (University of California, San Francisco) with ff99bsc0_chiOL3 RNA and ionsjc_tip3p ion forcefields. Charges of the DU177 RNA were neutralized by an appropriate number of Na^+ and Cl^- counter ions with (for production runs) or without 20 mM Mg^{2+}.

To construct the intermediate structure with formed stem S1 and partially formed stem S2 for the subsequent folding simulations, we used targeted molecular dynamics (TMD) simulations (35) to guide the ribose-phosphate backbones of stem S1 of DU177 (PDB ID: 2K96) to reshape into the isolated hairpin HP1 structure (PDB ID: 1NA2) (Supplementary Movie S4, first part). Next, the 6 nucleotides from the 3 terminal base pairs of stem S2 and the last three nucleotides (CUC) of loop L1 were TMD-guided to fold back to the corresponding regions of DU177 (Supplementary Movie S4, second part). In both TMDs, Mg^{2+} ions were omitted to increase the structural flexibility and facilitate conformational reshaping.

To simulate the TER folding pathway (see Figure 8C for a schematic of the indicated folding pathways), the intermediate structure was heated from 0 K to 310 K and then equilibrated for 10 ns in the presence of Mg^{2+}; backbones of the 3 terminal base pairs of stem S2 were restrained during this period. The system was then allowed to make a production run for 100 ns at a 2-fs time step without any restraint. The cutoff distance of non-bonded interactions was set to 10 Å. All temperature regulations were done using Langevin thermostat with a collision frequency of 2 ps^{-1}.

The same procedure was also applied to the INT pathway, except an additional TMD was carried out to reshape the 4 internal base pairs, instead of the 3 terminal base pairs, of stem S2 before the production run.

For the REM pathway, the first two nucleotides of stem S1 were mutated from GG to UU using the ModeRNA server (58). The resulting conformer (equivalent to $DU177^{S1\text{-}2m}$) was equilibrated for 100 ns without Mg^{2+} and restrained to relax the terminal end of stem S1. After restoring the two mutated nucleotides (UU to GG), the relaxed conformer was allowed to equilibrate for 10 ns in the presence of Mg^{2+} with both stems S1 and S2 restrained. Finally, the restraint was removed to let these two stems refold freely for a production run of 100 ns. Supplementary Movies S1–S3 show the first 10 ns of refolding; no apparent structural changes were found for the remaining 90 ns.

RESULTS

Folding of DU177 occurs through the intermediate hairpin HP1

We used optical tweezers (Supplementary Figure S1A) to study the folding and unfolding dynamics of DU177 RNA (Figure 1). Tension was applied to the two ends of the RNA molecule, which was then pulled by gradually increasing the force to unfold ('force-ramping' experiments). Figure 2A shows five typical pulling force-extension curves, each of which exhibits an apparent transition, corresponding to unfolding of the structure and characterized by the unfolding force and the extension change. Figure 2B summarizes 561 transitions appearing in three clusters, suggesting that the DU177 sequence can fold into at least three distinct conformations. Similar distribution patterns also have been previously identified (22,40). The 'HP' (hairpin) cluster corresponds to the independently formed stem S1-loop L1, because both the unfolding force and extension change of this cluster are indistinguishable from those measured from the isolated hairpin HP1 (Figure 4A and Supplementary Table S1). A curve based on the extensible worm-like chain model (50) was plotted on Figure 2B to predict the transitions consistent with unfolding of the DU177 pseudoknot. This curve passes through the 'high PK' (high-stability pseudoknot) and 'low PK' (low-stability pseudoknot) clusters, suggesting that they share a similar pseudoknot fold. Nevertheless, the low PK species is far less stable than the high PK species (unfolding force: 15.0 pN versus 43.0 pN), and thus the low PK species was proposed to be a folding intermediate with partially formed stem S2 (see below) (22). In our single-molecule measurements, the high PK species (corresponding to the native pseudoknot conformation) was present only in a small population (11.2%; Figure 2E, top), far from a homogeneous sample prepared for structural determination (38). The resultant structures of DU177 appear to be dependent on the folding pathways. Here, we applied some experimental strategies to the optical tweezers to tackle the RNA folding dynamics and pathways.

Stems S1 and S2 are two major secondary structures of the DU177 pseudoknot. By comparing the stability (unfolding force) of isolated hairpins (HP1 and HP2; Figure 1), Chen et al. found that HP1 had a higher unfolding force than HP2, and thus proposed that folding of DU177 follows the pathways of stem S1 (HP), a partially folded pseudoknot (low PK), and the fully-folded native pseudoknot (high PK) (22). We observed a similar trend of unfolding forces for these two isolated hairpins (Figure 4A). Moreover, when the imposed force was gradually decreased to allow the unfolded RNA to refold, we found that HP1 refolded at a higher force (thus faster) than HP2 (with refolding forces of 6.4 pN and 4.2 pN, respectively; Figure 4B). These results further support the notion that the major folding pathway of DU177 is initially done through the formation of stem S1, and thus hairpin HP1 is the dominant folding intermediate.

Pseudoknot folding is retarded by pre-formed HP1

By itself, hairpin HP1 contains six extra base pairs (including 4 non-canonical ones; see Figure 1) extended from stem S1 (59,60). All six base pairs must be opened and rearranged to form stem S2 and the major groove base triples of the pseudoknot (Supplementary Figure S2). Thus, this 'stem S1-first' folding pathway will encounter a high energy barrier that slows down the following reaction. To facilitate this reaction, we added 10 s of incubation time, during which the force was maintained at the lowest value (2 pN), for each unfolding-refolding cycle. Given the extra time for RNA refolding, the native pseudoknot population increased from 11.2% to 16.2% (Figure 2E and Supplementary Figure S1B), yet the overall pseudoknot formation efficiency remained low. This result suggests that the base-pair rearrangement of HP1 to form native pseudoknots was extremely slow and thus the RNA was likely trapped in a folding intermediate.

To further analyze the folding process of DU177, we did 'force-drop' experiments (61). The force imposed on the RNA was quickly dropped from the highest value (~45 pN when the RNA was completely unfolded) to a preset one (9–10 pN). Meanwhile, the folding process was monitored in real time by the extension change of RNA. As shown in Figure 5A, three apparent folding states, which always appeared in the same chronological order, were identified: unfolded, hopping, and steady (folded) states. The unstructured RNA took an average of 7.2 s (rate constant k_{fit} = 0.143 s^{-1}) to fold into the hopping state, which lasted 23.4 s (k_{fit} = 0.033 s^{-1}) before transitioning into a steady state (at 9 pN; Figure 5D and Supplementary Table S2). Structures of the hopping and steady states were further determined by increasing the force to measure their unfolding transitions, which were then compared with those of known structures (61). The results show that the hopping state was caused by the conformational interchange between HP1 and low-stability pseudoknots, and the steady state corresponded with the native pseudoknot (Supplementary Figure S3). In other words, HP1 went through many cycles of folding attempts via partially-folded or mis-folded pseudoknots to eventually pass the high energy barrier and form the native conformation. Thus, a moderate tension maintained at 9–10 pN appeared to facilitate pseudoknot formation by destabilizing these folding intermediates, which would be otherwise trapped when the force was decreased (as in the force-ramping experiments).

Masking part of the downstream sequence greatly facilitates pseudoknot formation

By using the full-length DU177, we demonstrated that folding of the sequence into native pseudoknots is a slow process. However, *de novo* synthesized RNA can start to fold as soon as a sufficient length has emerged from the surface of the RNA polymerase. Similarly, the upstream sequence of an mRNA structure can start to refold when it is unwound and emerges from the ribosome during translation. In both cases, the initial folding of RNA does not involve its downstream (3′ end) sequence. To test whether this can affect the outcome of DU177 folding, we extended the DNA handle into the 3′ end of the DU177 sequence to base-pair with its last two nucleotides, which would otherwise be involved in forming the last 2 bp of stem S2. The construct was named $DU177^{S2\text{-}2h}$ ('h' strands for handle; Figure 1),

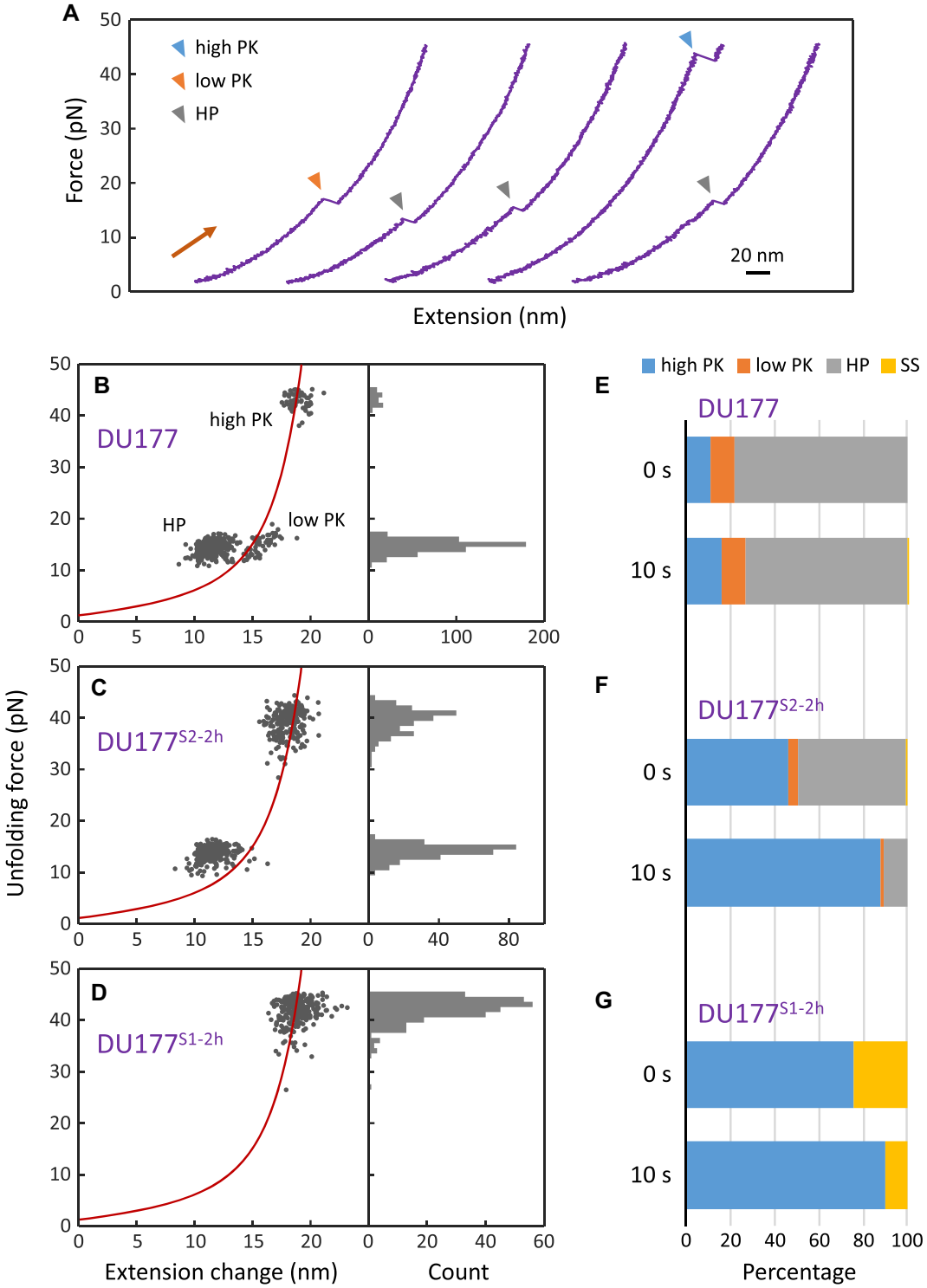

Figure 2. The availability of the upstream and downstream sequences determines the conformation of pseudoknot folding. (**A**) Representative force-extension curves. Shown are five consecutive pulling cycles from DU177. Transitions on the curve are indicated by triangles of specific colors, depending on their features: high-stability pseudoknots (high PK; blue), low-stability pseudoknots (low PK; orange), and hairpins (HP; gray). Distribution of the unfolding transitions of DU177 (**B**), DU177$^{S2\text{-}2h}$ (**C**), and DU177$^{S1\text{-}2h}$ (**D**) without extra incubation time (0 s) in folding cycles. The results acquired with 10 s of incubation time are shown in Supplementary Figure S1B. The dark red curves illustrate a worm-like chain model where the unfolding transitions from the intact pseudoknot to the single strand are expected to locate. The three distinct categories of transitions mentioned above are indicated. Populations of the transition categories for DU177 (**E**), DU177$^{S2\text{-}2h}$ (**F**), and DU177$^{S1\text{-}2h}$ (**G**) measured with (10 s) or without (0 s) extra incubation time. SS, single strands (not forming any apparent structures).

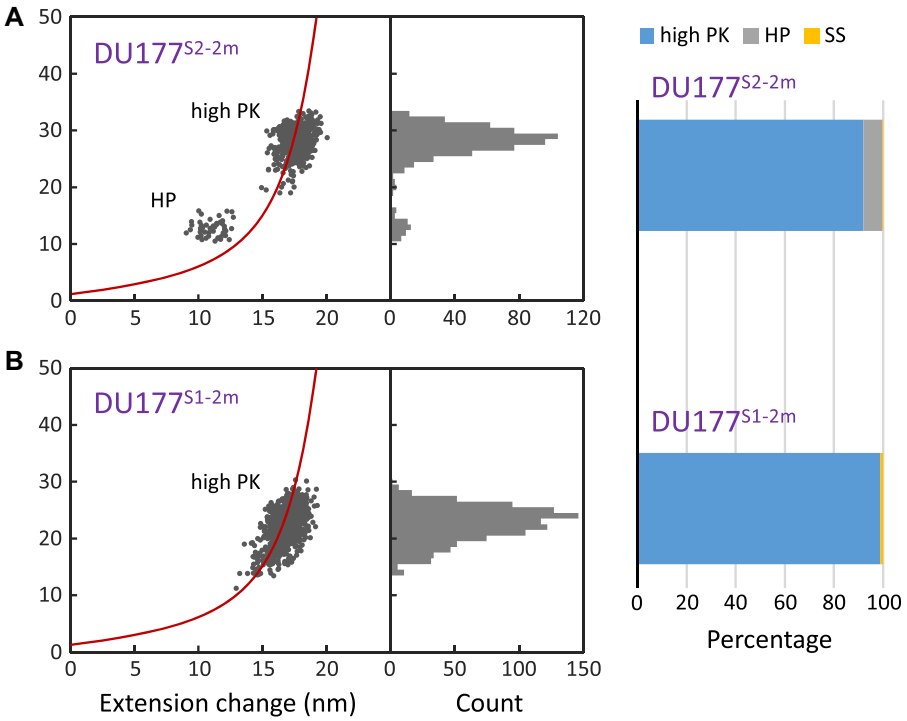

Figure 3. Pseudoknot stability is greatly affected by mutations in the upstream and downstream stems. Distribution of the unfolding transitions of DU177$^{S2\text{-}2m}$ (**A**) and DU177$^{S1\text{-}2m}$ (**B**). Both are from experiments with 10 s of incubation time in folding cycles. The dark red curves illustrate a worm-like chain model where the unfolding transitions from the intact pseudoknot to the single strand are expected to locate. Two distinct categories of transitions (high PK and HP) are indicated. Populations of the transition categories for each mutant are shown to the right. SS, single strands (not forming any apparent structures).

and it was used to mimic the RNA folding with temporary sequestering of a short downstream sequence by the ribosome or RNA polymerase. The results showed that, compared with the uncovered DU177, DU177$^{S2\text{-}2h}$ exhibited an increased probability of folding into the high-stability pseudoknot, and its population was dramatically increased from 11.2% to 46.3% or 16.2% to 87.7% (without or with an additional 10-s incubation time, respectively) (Figure 2C and F, and Supplementary Figure S1B). To further confirm that disrupting the last 2 bp of stem S2 can promote pseudoknot formation, we made the corresponding mutant DU177$^{S2\text{-}2m}$ ('m' stands for mutation; Figure 1), in which the last 2 nucleotides were mutated. As shown in Figure 3A, the population of pseudoknots was 92.0% in this mutant, comparable to that in DU177$^{S2\text{-}2h}$ (87.7%) under the same conditions. These results demonstrate that the pseudoknots folded in a much more efficient way when the last two nucleotides were not available during the folding process. In addition, the pseudoknot stability was decreased significantly from 42.4 pN (DU177) to 39.8 pN (DU177$^{S2\text{-}2h}$) to 28.4 pN (DU177$^{S2\text{-}2m}$) (Figure 4C and Supplementary Table S1), indicating that these two handle-sequestered nucleotides in DU177$^{S2\text{-}2h}$ were retrieved, but not thoroughly, back to the pseudoknot when the folding was completed.

Furthermore, we lengthened the DNA handle to cover the last four nucleotides from the 3′ end of DU177 (DU177$^{S2\text{-}4h}$, Supplementary Figure S4A). As with DU177$^{S2\text{-}2h}$, DU177$^{S2\text{-}4h}$ also showed enhanced pseudoknot forming efficiency of 29.5% or 68.1%, without or with an additional 10-s incubation time, respectively, and the unfolding force was further dropped to an average around 36 pN with a wide distribution (Supplementary Figure S4B–D). By contrast, the corresponding mutant, DU177$^{S2\text{-}4m}$, predominantly appeared in the hairpin conformation (89.8%), and high-stability pseudoknots were not detected (Supplementary Figures S4B, C). These results further support that DU177 has a higher propensity to fold into pseudoknots when its last few nucleotides (i) are not available temporarily during folding and (ii) can be at least partially retrieved before the folding is completed.

Next, we did force-drop experiments to monitor real-time folding of DU177$^{S2\text{-}2h}$. Like with DU177, DU177$^{S2\text{-}2h}$ folded into pseudoknots through an intermediate state (Figure 5B) with a rate constant of 0.093 s^{-1}, somewhat slower than that of DU177 (0.143 s^{-1}; Figure 5D and Supplementary Table S2). Unlike DU177, the intermediate of DU177$^{S2\text{-}2h}$ existed only in a stable state, corresponding to HP1, and the rate constant of pseudoknot formation from the intermediate was 0.080 s^{-1}, more than 2-fold faster than that of DU177 (0.033 s^{-1}; Figure 5D and Supplementary Table S2). These results clearly demonstrate that the very downstream sequence of DU177 was actively involved in the dynamic formation of mis-folded pseudoknots, and that folding can be redirected from the off-pathway to the on-pathway when the downstream sequence was not available.

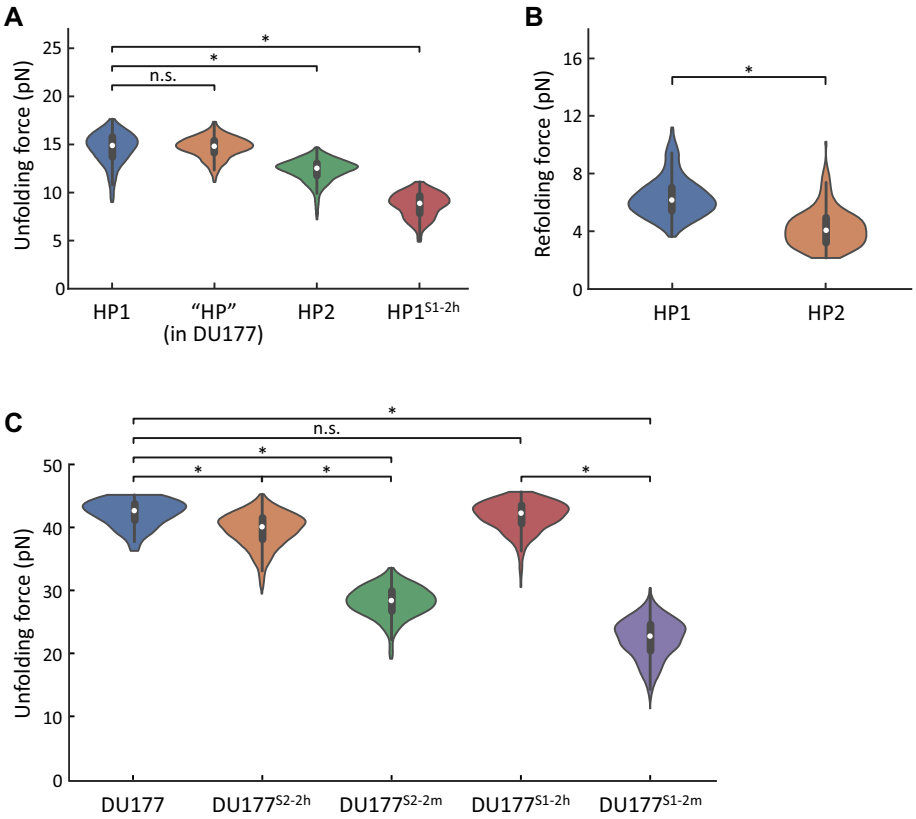

Figure 4. Distribution of unfolding and refolding forces. **(A)** Unfolding forces of isolated hairpin HP1, the 'HP' state from DU177 (see Figure 2B), isolated hairpin HP2, and $HP1^{S1\text{-}2h}$ (isolated HP1 with the two most-upstream nucleotides masked by the DNA handle). **(B)** Refolding forces of isolated HP1 and HP2. The refolding force is the force at which the RNA folds from the unstructured state into the hairpin state when the tension is gradually decreased in refolding cycles. **(C)** Unfolding forces of the 'high PK' states from DU177, $DU177^{S2\text{-}2h}$, $DU177^{S2\text{-}2m}$, $DU177^{S1\text{-}2h}$ and $DU177^{S1\text{-}2m}$. Data from experiments with 10 s of incubation time in folding cycles. Data are shown in violin plots; open circles represent the median; thick bars represent the range of the first and third quartiles; thin bars extend up to the extremes of the data within 1.5 times interquartile range on each side. Wilcoxon rank sum test was used for statistical testing; $*P < 0.05$; n.s., not significant.

Folding of native pseudoknots is optimally achieved through pre-formed stem S2

Since the availability of the downstream sequence can greatly influence the folding of DU177, the next question raised was whether the upstream sequence could have any effects. Therefore, we extended the upstream DNA handle into the 5′ end of the DU177 sequence by 2 bp to interfere with the formation of stem S1 ($DU177^{S1\text{-}2h}$; Figure 1). Surprisingly, $DU177^{S1\text{-}2h}$ either folded into high-stability pseudoknots (75.5%; Figure 2D and G) or failed to form any apparent structures (24.5%); no intermediates were detected. The folding efficiency of high-stability pseudoknots was increased to 90.0% with 10 s of incubation time (Figure 2G and Supplementary Figure S1B). A similar result was found in the corresponding mutant $DU177^{S1\text{-}2m}$ (Figures 1 and 3B). Thus, DU177 appeared to follow a different folding pathway when its first two nucleotides were not available, leading to the pseudoknot-or-none results. On the other hand, compared with the unmasked DU177, the unfolding force of the $DU177^{S1\text{-}2h}$ pseudoknot was statistically indistinguishable, whereas the $DU177^{S1\text{-}2m}$ showed a dramatic decrease by approximately 20 pN (Figure 4C and Supplementary Table S1). This big force drop in $DU177^{S1\text{-}2m}$ (for comparison, it was 14 pN in $DU177^{S2\text{-}2m}$; see above) suggests that the equilibrium from the pseudoknot missing the first 2 bp toward the native conformation was highly favored and thus, in $DU177^{S1\text{-}2h}$, the pseudoknot could outcompete with the handle for the two shared nucleotides to retain the same stability as the native DU177.

After masking the first two nucleotides at the 5′ end, the folding of stem S1 was greatly impaired. This was demonstrated by a control experiment with $HP1^{S1\text{-}2h}$ (the isolated hairpin HP1 with the same 5′ end handle extension of $DU177^{S1\text{-}2h}$). The unfolding force of $HP1^{S1\text{-}2h}$ dropped from 14.6 pN (when unmasked) to 8.7 pN (Figure 4A and Supplementary Table S1). This force was even lower than that of HP2 (12.3 pN; Figure 4A), another secondary structural component of the pseudoknot, suggesting that stem S2 formed prior to the masked stem S1 during the folding of $DU177^{S1\text{-}2h}$, i.e., the 'stem S2-first' pathway was followed. Note that, unlike $DU177^{S1\text{-}2h}$, the isolated hairpin counterpart $HP1^{S1\text{-}2h}$ apparently lost the capability to retrieve the handle-sequestered nucleotides, because this hairpin lacks the key base triples found in the pseudoknot structure (see the results for U3C below).

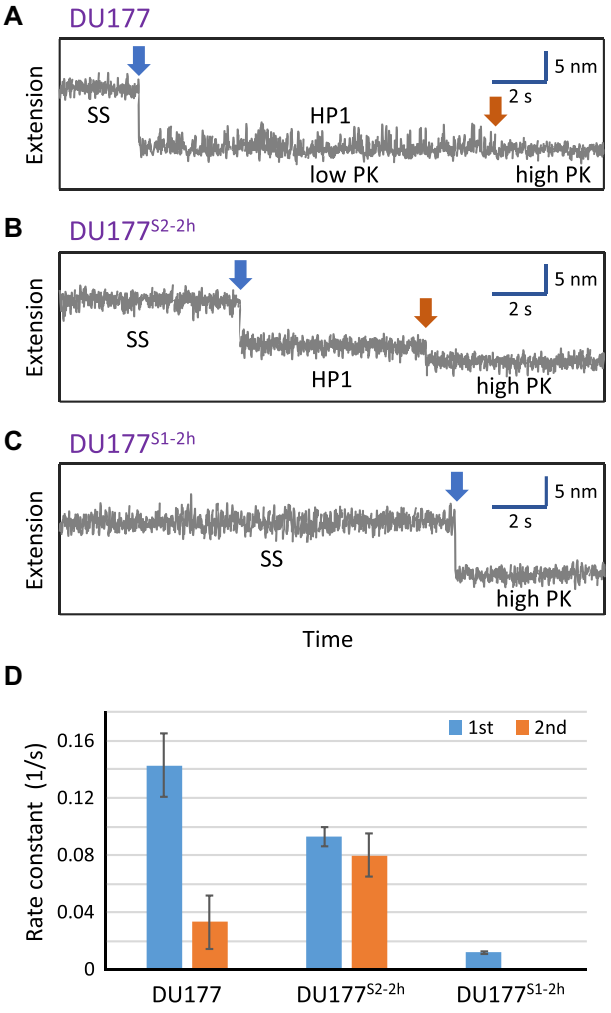

Figure 5. The availability of the upstream and downstream sequences determines pseudoknot folding kinetics. Force-drop experiments were applied to follow the folding process (time-evolved extension changes) of DU177 (**A**), DU177$^{S2\text{-}2h}$ (**B**) and DU177$^{S1\text{-}2h}$ (**C**) from the single-stranded (SS) state to a folded state (HP1, low PK, or high PK). The force was maintained at 9 pN in these examples. One or two apparent conformational transitions (indicated by blue or orange arrows) were observed from the traces. The folded structure at the end was determined by ramping the force to examine its unfolding transition (see Supplementary Figure S3). (**D**) Rate constants (k_{fit}) of the first (blue) and second (orange) conformational transitions described above. Note that only one apparent transition was detected in DU177$^{S1\text{-}2h}$. Error bars represent 95% confidence intervals. See Supplementary Table S2 for details.

As opposed to the two-step folding pathway of DU177 and DU177$^{S2\text{-}2h}$, DU177$^{S1\text{-}2h}$ folded into its pseudoknot conformation in one apparent single step (Figure 5C) with a rate constant of 0.011 s^{-1}, approximately one order of magnitude slower than the first step (formation of stem S1) of its counterparts (DU177 and DU177$^{S2\text{-}2h}$) (Figure 5D and Supplementary Table S2). As discussed above, with the impaired stem S1 formation capability, DU177$^{S1\text{-}2h}$ would begin to fold with stem S2, whereby the rate would be compromised. However, as soon as stem S2 formed, folding of the remaining upstream sequence was greatly accelerated because this reaction would result in extensive hydrogen bond formation (including three major groove base triples, two minor groove base triples, and one Hoogsteen base pair) without breaking any existing base pairs of stem S2 (an enthalpy-driven reaction; Supplementary Figure S2). Thus, the pseudoknot could fold quickly and correctly following the formation of stem S2. This folding mechanism can account for the pseudoknot-or-none result of DU177$^{S1\text{-}2h}$.

Because the sequence from the DNA handle (acting in *trans*) greatly influenced the RNA folding, we then tested whether the flanking sequence from the same RNA strand (acting in *cis*) could also play a role. We inserted a 49-nucleotide linker between the 5′ handle and the pseudoknot (DU177^{Linker49nt}; Supplementary Figure S5A). The results show that the population of high-stability pseudoknots was increased to 44.0% (compared to 11.2% in DU177; Supplementary Figure S5B and C). This was likely caused by the formation of potential structures involving the linker and the upstream region of stem S1 (Supplementary Figure S5A); this structure would impede the formation of stem S1 and thus facilitate the stem S2-first folding pathway. Accordingly, different sequences flanking either the upstream or the downstream of the structure may influence its folding to different extents.

Refolding of the full DU177 pseudoknot is correlated with frameshifting efficiency

We have previously shown that the three major groove base triples in the DU177 pseudoknot act as the core for the formation of other tertiary base pairs and enhance the unwinding resistance (and thus the integrity) of stem S1 (40). Here, we argue that this structural coordination was the driving force to restore the full length of stem S1 during the folding of DU177$^{S1\text{-}2h}$. To test this hypothesis, we made a mutant, U3C, in which the three major groove base triples of DU177 were disrupted (Figure 1) (22). As in DU177, the folded structures of U3C were also distributed in three apparent groups, but the corresponding high-stability pseudoknot exhibited a lower unfolding force of 24.4 pN and a higher population of 43.2% (Figure 6A and Supplementary Table S1) (22). These results indicate that U3C could form pseudoknots more efficiently but, due to the lack of the major groove base triples, the structural stability was greatly decreased. Remarkably, when the first two nucleotides on the 5′ end were sequestered by the handle, U3C$^{S1\text{-}2h}$ failed to form any high-stability pseudoknots (Figure 6B). This result suggests that this construct has greatly lost the capability to retrieve nucleotides from the handle and explains, at least in part, the low frameshifting efficiency by U3C (3%) (22).

As shown above, DU177 and U3C respectively demonstrate the strong and weak nucleotide-retrieval capability from the 5′ handle. Besides, they also represent the two extremes of frameshifting efficiency in a series of mutants: 53% and 3% for DU177 and U3C, respectively (22). Therefore, a correlation between nucleotide retrieval and frameshifting efficiency seems to exist in this case. To test, we chose another mutant UUC, which is a loop L2 mutant (Figure 1) and has a modest frameshifting efficiency of 22% (40). As in our previous findings (40), UUC folded mainly into the high-stability pseudoknots (81%; Figure 6C and E). When the first two nucleotides of the pseudoknot

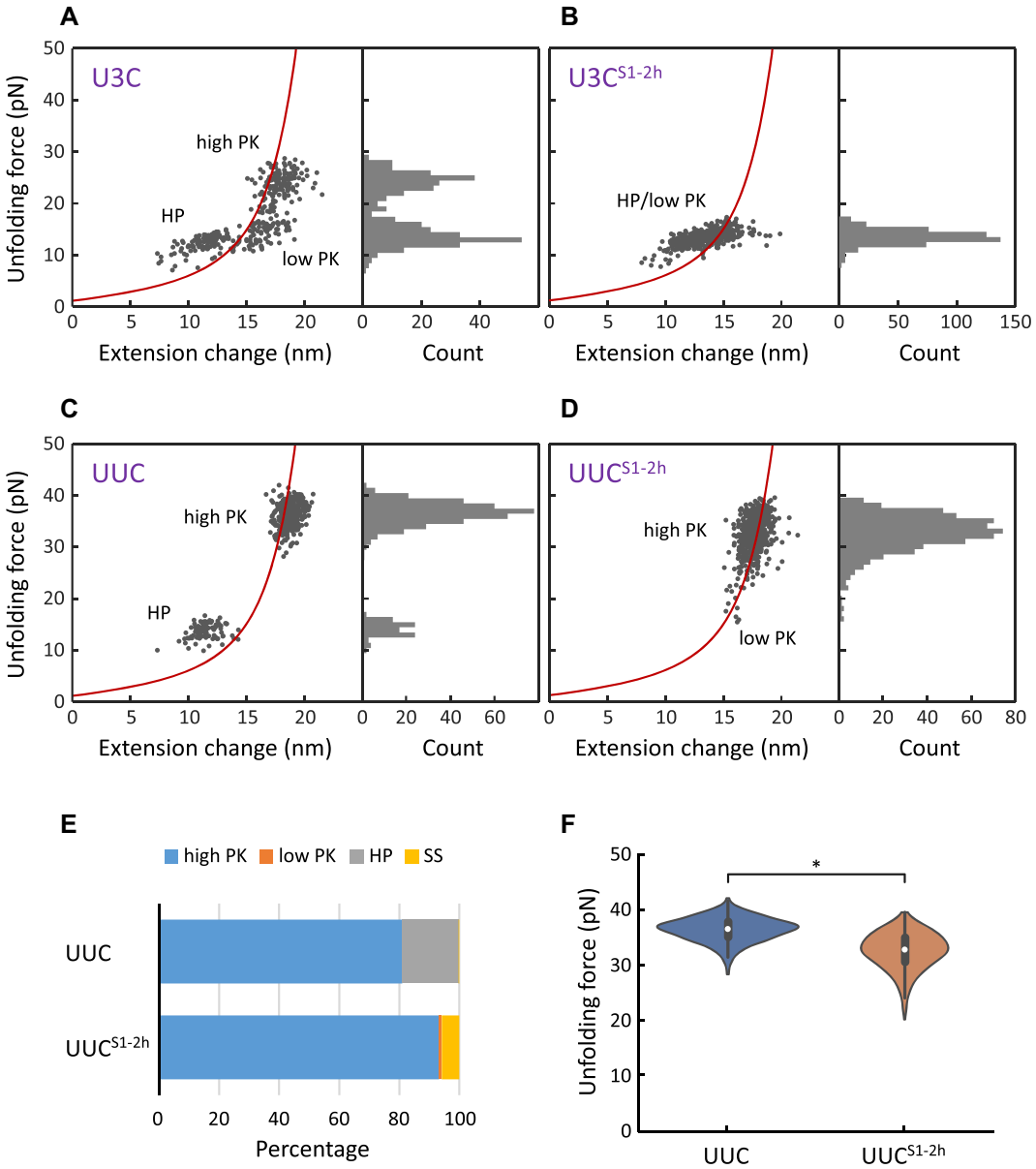

Figure 6. The upstream stem is not stabilized when key structural components inside the pseudoknot are disturbed. Distribution of the unfolding transitions of U3C (**A**), U3C$^{S1\text{-}2h}$ (**B**), UUC (**C**), and UUC$^{S1\text{-}2h}$ (**D**). All are from experiments with 10 s of incubation time in folding cycles. The dark red curves illustrate a worm-like chain model where the unfolding transitions from the intact pseudoknot to the single strand are expected to be located. Three distinct categories of transitions (high PK, low PK and HP) are indicated. Note that, in U3C$^{S1\text{-}2h}$, the high PK population was not observed and the boundary between the HP and low PK populations is not clear. (**E**) Populations of the transition categories for UUC and UUC$^{S1\text{-}2h}$. (**F**) Distribution of unfolding forces from the high PK populations of UUC and UUC$^{S1\text{-}2h}$. Wilcoxon rank sum test was used for statistical testing; $*P < 0.05$.

were sequestered, UUC$^{S1\text{-}2h}$ appeared exclusively in pseudoknot conformations (Figure 6D and E), consistent with the stem S2-first folding pathway as in DU177$^{S1\text{-}2h}$. Moreover, the unfolding force of the high-stability pseudoknots was decreased modestly from 36.6 pN (UUC) to 32.7 pN (UUC$^{S1\text{-}2h}$), but the difference was statistically significant (Figure 6F and Supplementary Table S1), suggesting that UUC$^{S1\text{-}2h}$ could retrieve the handle-sequestered nucleotides but not completely. In other words, these two shared nucleotides may reach a fast equilibrium of interchange between the pseudoknot and the handle, and thus the pseudoknot stability was compromised. Thus, these results support the positive correlation between the nucleotide retrieval rate and frameshifting efficiency for these studied DU177 constructs.

Pseudoknots with enhanced stem S1 are resistant to ribosomal unwinding

Ribosomal frameshifting is greatly enhanced by stimulatory mRNA structures. Exploring how the structure reacts in response to translocating ribosomes is essential to understanding the molecular mechanism of frameshifting. Given that stem S1 of an RNA pseudoknot is the first

structural moiety targeted by ribosomes during translation, we investigated the conformational changes in pseudoknots with a stabilized (DU177) or unstabilized (U3C) stem S1 when the ribosome was stalled upstream. These experiments were done using single-molecule Föster Resonance Energy Transfer (smFRET). The mRNA was designed to contain several unique codons where the ribosome can be specifically stalled to interact with the downstream pseudoknot to different extents (Figure 7A). Cy3 and Cy5 dyes were labeled in loops L1 and L2 of the pseudoknot, respectively. The conformations of the structure under the action of ribosomes could be reflected by FRET efficiencies (E_{FRET}). The results show that U3C exhibited the same E_{FRET} peak (at ∼0.59) when present alone ('PK alone'; Figure 7C, bottom) or when forming initiation complexes with ribosomes ('M'; Figure 7C), in which the mRNA entrance site of the ribosome was expected to cover up to the position at approximately +14 (62,63), about 1 nucleotide away from the structure (see Figure 7A). However, a low E_{FRET} peak (∼0.4) started to appear when the ribosome had translocated to the third ('MFK'; Figure 7C) or fourth codon ('MFKE'). This low E_{FRET} peak corresponded to the conformation of isolated HP2 ('HP2'; Figure 7B and C, bottom). Thus, U3C lacking the major groove base triples underwent an apparent one-step structural transition from the pseudoknot to HP2 when stem S1 was unwound by translocating ribosomes. By contrast, when DU177 was translated, a high E_{FRET} peak (∼0.7) emerged immediately when the ribosome translocated to the second codon ('MF'; Figure 7D), and the low peak corresponding to the HP2 conformation became apparent only after translocation to the fourth codon ('MFKE'; Figure 7D). This unique 0.7 E_{FRET} peak, not observed in U3C, likely reflected a distorted pseudoknot conformation due to the unwinding resistance of base-triple-stabilized stem S1 in DU177. This viewpoint was supported by our recent results in steered molecular dynamics (SMD) simulations (35). Loop L2 of the DU177 pseudoknot was shown to dock on the positively charged ribosomal protein uS3 at the entrance site, such that loop L1 was pulled closer (and thus exhibited a higher FRET efficiency) when the translocation proceeded (35). In fact, binding between the mRNA backbone and uS3 at the entrance site has also been reported in recent structural studies (64,65). Thus, the unfolding of DU177 pseudoknots by ribosomes was likely mediated by a stable intermediate structure prior to the complete opening of stem S1.

DISCUSSION

Based on our single-molecule data, we developed a model (Figure 8A) to illustrate the potential folding pathways of DU177. The structural formation begins with stem S1 predominantly, at a folding rate about 10 times faster than stem S2 (Figure 5D). The initially formed stem S1 contains 6 extra base pairs in loop L1 (Figure 1), which must be disrupted before subsequent stem S2 folding. Thus, this is a slow process. Meanwhile, intermediates that involve limited base-pairing with the most-downstream sequence form quickly and reversibly (corresponding to the hopping state; Figure 5A) and tend to be kinetically trapped. Therefore, masking the downstream sequence suppresses the formation of intermediates (Figure 5B) and greatly promotes the formation of native pseudoknots (Figure 2F). On the other hand, the folding of DU177 starts from stem S2 at a slower rate when the most-upstream nucleotides are masked. As soon as stem S2 forms, the successive folding occurs instantly (Figure 5C), because it requires no disruption of existing base pairs and results in the formation of several base triples that stabilize the whole structure (Supplementary Figure S2). This model demonstrates that the pathway, kinetics, and outcome of pseudoknot folding can be affected significantly by the availability of an extremely short sequence (down to 2 nucleotides) at the very beginning or end of the structure.

The data acquired from optical tweezers are mainly time-evolved force and extension trajectories of the tether, and thus assignments of structural transitions and dynamics will highly rely on the knowledge available for the molecule of interest, such as secondary and tertiary structures and thermodynamics. In general, the known information is not sufficient to account for all measured results, and thus some inference we have drawn here may need further confirmation.

Figure 8A shows that the RNA folding can take an alternative route if the most-stable secondary structural component is destabilized (as in $DU177^{S1\text{-}2h}$). This finding is consistent with a recent study for VPK, a variant of the frameshift-stimulating pseudoknot from the mouse mammary tumor virus (MMTV) (66). The VPK pseudoknot follows the dominant stem S1-first folding pathway (stem S1 is more stable than S2), but a parallel stem S2-first pathway appears when stem S2 becomes stable after increasing the salt concentration (66). An earlier study by Cho et al. also showed a similar result (67). The authors compared the folding of three RNA pseudoknots [including DU177, VPK, and the frameshift stimulator from the simian retrovirus type 1 (SRV-1)] with similar contact maps and found that the relative stabilities of the constituent secondary structures (stems) predominantly determine the order of their assembly into the pseudoknot (67); in principle, the more stable one folds first. Thus, it may be a general feature for some RNA pseudoknots that their folding pathway can be altered by modulating the stabilities of their constituent structures.

The folding dependence on the availability of downstream sequences has a significant impact on the function of frameshift-stimulating RNA pseudoknots. Located within the coding region of mRNA, the pseudoknot is unfolded repeatedly by consecutive translating ribosomes and shall start to refold before its downstream sequence has emerged entirely from the exit site of the ribosome. Therefore, the formed structures can be different and thus have different frameshift-stimulating capabilities for the upcoming ribosomes, a phenomenon similar to that observed in polysomes (68). In other words, the frameshifting efficiency of an mRNA template can be mediated by the relative translation rate of the preceding ribosome that just passes through the RNA pseudoknot. This hypothesis explains, at least in part, why frameshifting efficiencies measured for the same frameshift signal can vary significantly under different experimental systems. For example, the reported efficiency for the frameshift signal from severe acute respi-

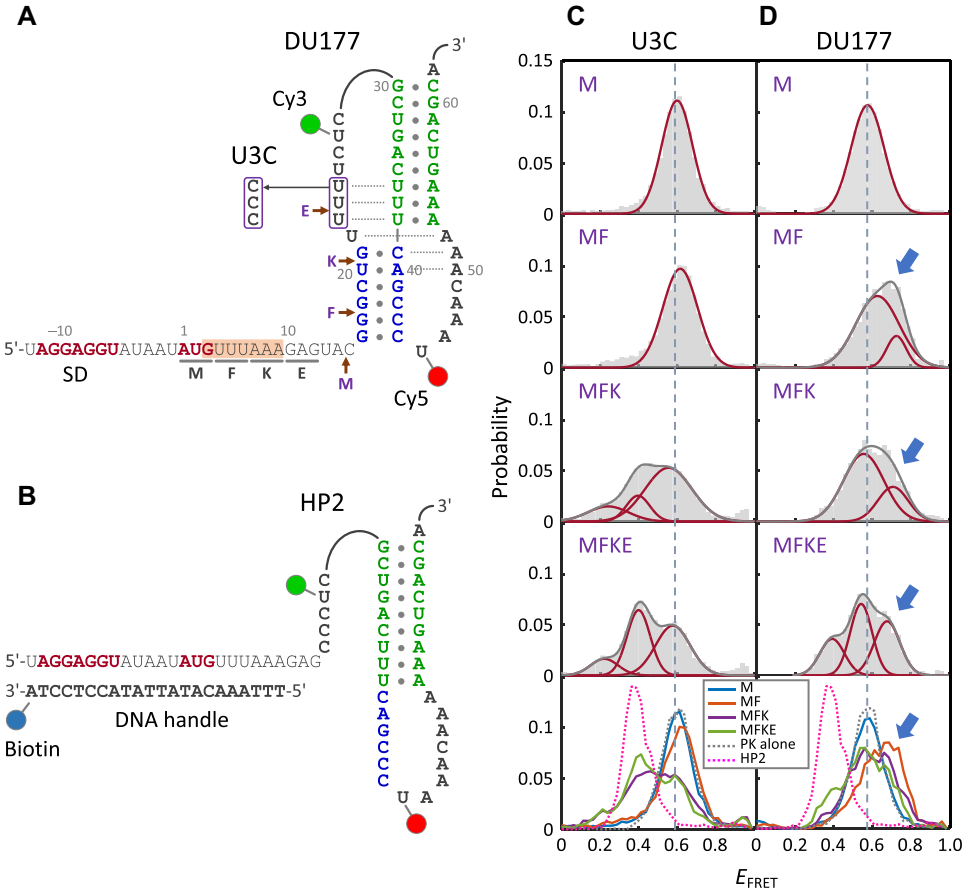

Figure 7. Pseudoknots with enhanced stem S1 are resistant to ribosome unwinding. (**A**) Design of mRNA for smFRET experiments. The first four codons (M, F, K, and E) are underlined. Expected boundaries of the mRNA entrance site are indicated by arrows when the P site of the ribosome is located at the designated codons. The illustrated pseudoknot is from DU177; the mutated nucleotides in U3C are indicated. The position for a heptameric slippery site is shaded in orange (Note that the sequence used here is not a slippery sequence). A Cy3 and a Cy5 dyes are labeled in loop L1 and L2 of the pseudoknot, respectively. SD, the Shine-Dalgarno sequence. See Figure 1 for other annotations. (**B**) Design of the HP2 construct. Part of the DU177 pseudoknot is deleted and the hairpin 2 region remains intact. A complementary, biotin-labeled DNA handle is annealed to the upstream region for smFRET measurements. The same DNA handle is annealed to the mRNA shown in (A) to make the 'PK alone' constructs. (**C**) Histograms of E_{FRET} of U3C when it is translated by ribosomes to the indicated codons. Each histogram is fit by one to three Gaussian functions (red curves) that best describe the distribution. For more clarity and a better comparison, all histograms are also plotted in line curves in the bottom panel, where the data from the ribosome-free samples ('PK alone' and HP2) are also shown. (**D**) Same as in (C), except that DU177 mRNA was used. A unique high E_{FRET} population (~0.7) appearing in DU177 but not in U3C was indicated by arrows.

ratory syndrome coronaviruses (SARS-CoV) ranges from ~3% in yeast, ~15% in both epithelial cells and rabbit reticulocyte lysates, to ~24% in wheat germ lysates (69), and up to 60% in a coupled transcription-translation cell-free system (70).

What conformations are the folding intermediates shown in Figure 8A? Given the available sequence in the loop of preformed stem S1 and the involvement of the most-downstream sequence, we hypothesize that folding of the major intermediates starts from the terminal 3 bp of stem S2, which then propagates sequentially by competing for the nucleotides paired in the extra 6 bp of preformed stem S1 (Supplementary Figure S6A). Formation of the whole 9-bp stem S2 requires that the two helical strands twist by almost one turn. However, the twisting is torsionally restrained, because one strand of the helix is confined within stem S1 and the other (involving loop L2) is A-rich and stiff (due to base stacking) (40). Thus, the folding tends to be stalled midway with a partially formed stem S2, resulting in torsionally restrained intermediates. This hypothesis is supported by our molecular dynamics (MD) simulations, which showed that only the terminal #2–#4 bp formed when the folding of stem S2 was constrained to begin from the terminal end (Figure 8C, 'TER'; Supplementary Figure S6B; Supplementary Movie S1). One way to mitigate the torsional hindrance is to promote the folding of stem S2 from within the internal region when the extra 6 bp of preformed stem S1 open transiently during breathing. This pathway can be promoted by masking the most-downstream sequences (as has been observed in DU177$^{S2\text{-}2h}$ and DU177$^{S2\text{-}4h}$) or by destabilizing the extra 6 bp (e.g. in U3C). In U3C, the 3 U*U base pairs (with two hydrogen bonds each) of this region were replaced by the less stable C*U base pairs (with 1 hydrogen bond each) (Figure 1) (40,59,60). Indeed, we found that the appearance of intermediates was decreased in U3C (56.8%; Figure 6A), compared to DU177 (83.6%; Figure 2E, bot-

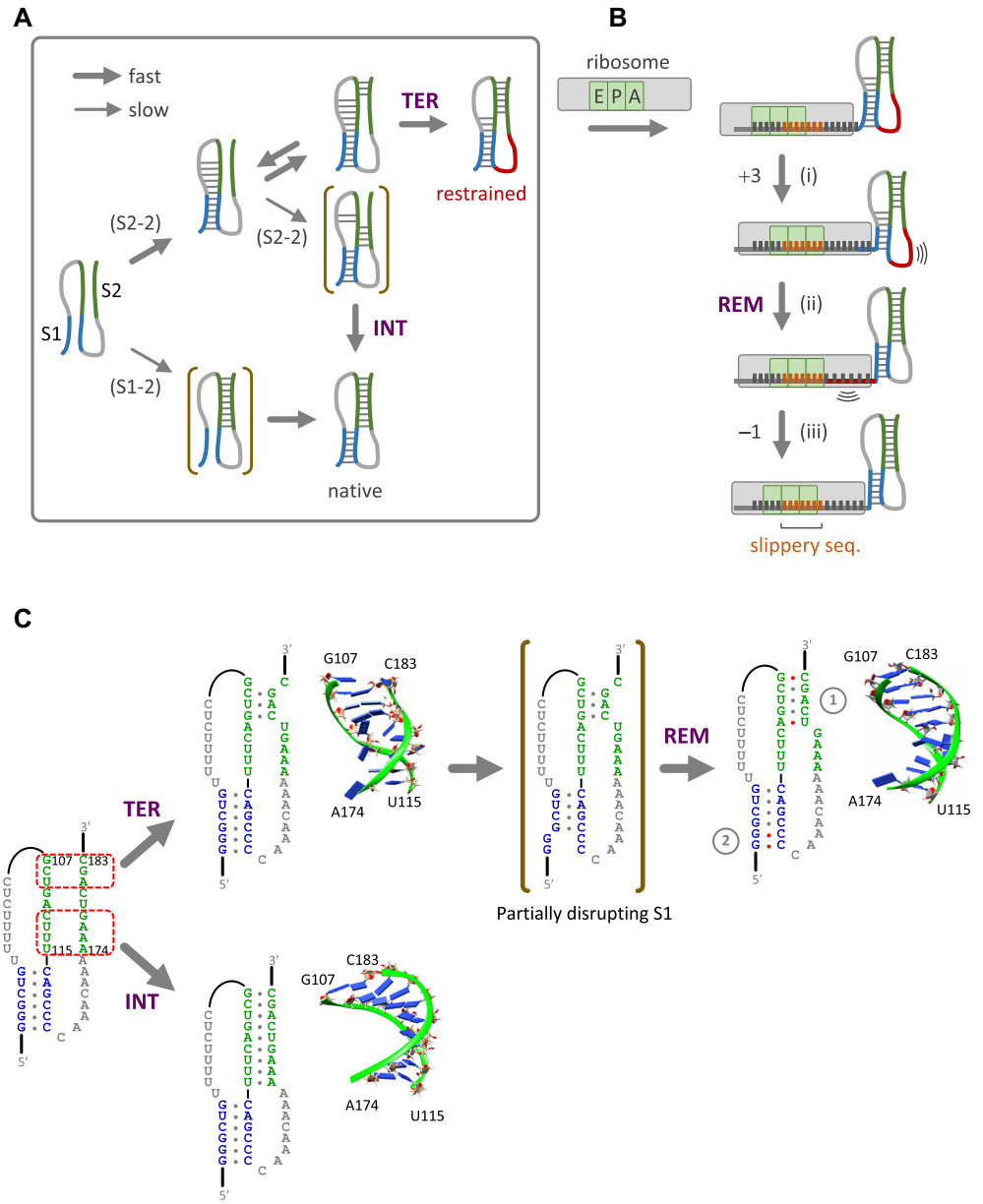

Figure 8. Pseudoknot folding pathways and remodeling. (**A**) Folding pathways of DU177 pseudoknots. Thick and thin arrows indicate relatively faster and slower reactions at each branching point. (S1-2) and (S2-2) indicate the major paths for DU177$^{S1\text{-}2h}$ and DU177$^{S2\text{-}2h}$, respectively. Transient folding intermediates are enclosed in square brackets. The putative torsionally-restrained region of major intermediates is shown in red. See Figure 1 for other color annotations. Base triples and Hoogsteen base pairs are not shown for clarity. (**B**) A hypothetical, interactive model for –1 ribosomal frameshifting. When the ribosome translocates into the upstream region of the low-stability intermediate structure (i), remodeling of the structure is induced to occur. The refolded pseudoknot restores its native mechanical strength to retrieve the ribosome-occupied sequence, resulting in stretching of the mRNA strand inside the ribosome (ii). After accommodation of the A-site tRNA (not shown) to the slippery sequence, the ribosome may slip backward to the –1 frame before translocation to the next codon (iii). The ribosome is shown in schematic; the three tRNA-binding sites (E, P, A) are indicated. (**C**) MD simulations. The molecular model (left) with paired stem S1 and unpaired stem S2 was built from the DU177 pseudoknot (PDB ID: 2K96), by TMD simulations. This model was used as the starting structure for the following MD simulations. Stem S2 was promoted to fold freely from its terminal end (TER) or its internal region (INT) after an initial constraint on the ribose-phosphate backbones of the corresponding nucleotides (dashed red boxes). The folded product from the TER route was subjected to disrupting the first 2 bp of stem S1 and then allowed to refold again (REM). The results show that two additional base pairs (red dots, marked '1') were formed, followed by reformation of the disrupted base pairs (red dots, marked '2'). Structures (the stem S2 region only) after production runs of MD simulations are shown to the right of each schematic presentation. Nucleotides are numbered per the original DU177 sequence (38). The indicated 'TER' and 'INT' steps in (A) and the 'REM' step in (B) correspond to the same steps in (C).

tom). MD simulations also showed that the whole stem S2 formed quickly when folding was constrained to begin from the internal region (Figure 8C, 'INT'; Supplementary Figure S6B; Supplementary Movie S2). Another way to mitigate the torsional hindrance during the folding of stem S2 is to increase the compliance of loop L2, for example, by substituting U's or C's for the A's to minimize base stacking. This was demonstrated by the UUC construct (Figure 1), in which the formation of intermediates was greatly suppressed to only 18.8% (Figure 6C and E). Overall, the above experimental data support the hypothesis that the major intermediate conformation of DU177 is a kinetically-trapped, torsionally-restrained pseudoknot with an incomplete stem S2.

As mentioned earlier, the DU177 pseudoknot is originally derived from the human telomerase RNA (38). Although this pseudoknot is not from an mRNA sequence, its key secondary and tertiary structural features involved in frameshifting, such as the G/C-rich stem S1 (5–6 bp), the A-rich (base-stacking) loop L2, and the major/minor groove base triples, are shared with the frameshift-stimulating pseudoknots from some viruses, including SRV-1 and the beet western yellow virus (BWYV) (39,40). In general, the RNA structure plays a more important role than the sequence in frameshift stimulation. For example, the MMTV pseudoknot and its variant VPK showed the same frameshifting efficiency of 12% (71); VPK differed from MMTV by flipping 4 G•C base-pairs in the stems (thus 8 nucleotides were different in the sequence) but did not appear to change the conformation. By contrast, another variant APK showed an extremely low frameshifting efficiency of 2% (71); APK differed from VPK by only two nucleotides in stem S2 but exhibited very different conformations (72,73). Thus, structural features identified from DU177 still can provide a mechanistic insight into how an RNA structure stimulates ribosomal frameshifting.

An increasing number of studies have shown that RNA structures stimulate frameshifting more efficiently if they have a higher propensity to fold into intermediate conformations (termed conformational plasticity or heterogeneity) (23–30). This propensity can be quantified as the conformational Shannon entropy, which was shown to correlate linearly with frameshifting efficiency in a force range relevant to the action of the ribosome (31). However, the underlying mechanism remains unclear. Here, we provide some evidence that briefly explain why conformational plasticity is important. As shown in Figure 8B, when the ribosome translocates into the torsionally-restrained intermediate, the terminal 1–3 bp (depending on the frame) of stem S1 will be unwound, because the intermediates are mechanically unstable and unlikely to tolerate ribosomal unwinding. The partial unwinding of stem S1 can relieve the restraint on stem S2 and allow its stalled folding to resume. This conformational remodeling is supported by our MD simulations (Figure 8C, 'REM'; Supplementary Figure S6B; Supplementary Movie S3). Such reorganized conformation of the pseudoknot is similar to the folding intermediate of $DU177^{S1\text{-}2h}$, both with sequestered most-upstream nucleotides and completely folded stem S2. Thus, the stability of stem S1 will be enhanced to retrieve the otherwise ribosome-occupied nucleotides, resulting in stretching of the mRNA strand inside the ribosome, which can potentially cause frameshifting as proposed previously (32–35). The importance of stem S1 stability, especially from its terminal end, is supported by the observation that the stability of the first 3–4 bp of the human immunodeficiency virus type 1 (HIV-1) hairpin was positively correlated with frameshifting efficiency (20). In line with the concept of conformational plasticity, we hypothesize that the pseudoknot remodeling from an intermediate, rather than the presence of a preformed native structure, is a more effective way to create mRNA stretching inside the ribosome.

This putative ribosome-induced pseudoknot remodeling is analogous to the action of RNA chaperones (1,8,11,12), where trapped folding intermediates are rescued by interaction with RNA binding proteins and redirected to the formation of native conformations. Indeed, the ribosome has been shown to chaperone folding of T4 thymidylate synthase group I intron by translating the pre-mRNA to resolve the aberrant base pairing initially formed between the intron and the upstream exon (74–76).

According to our model, conformational plasticity is a necessary but not sufficient feature for a high-efficiency frameshifting stimulator; having the capability to refold from an intermediate into a high-stability structure to compete with ribosomes for the occupied nucleotides is also required. This argument is supported by reinspection of the previous single-molecule study for a series of DU177 mutants (22). Looking closely at the reported unfolding force distribution (see Figure 4 of reference (22)), we can determine that intermediates are the dominant population (mostly greater than 50%) for each of the DU177 variants, but their frameshifting efficiencies can vary from ∼0% to 53%. However, when the population with higher unfolding force is considered, the forces are positively correlated with frameshifting efficiencies (22), highlighting the importance of the most stable structure that an RNA variant can fold. These features are concluded from the study of DU177 pseudoknots; whether they are applicable to other frameshift-stimulating RNA structures warrants further investigation.

SUPPLEMENTARY DATA

Supplementary Data are available at NAR Online.

ACKNOWLEDGEMENTS

We thank Dr Harry Noller (UC Santa Cruz) for providing the *E. coli* KLF203 strain and the plasmids of IF1, IF2, IF3 and EF-G. We thank Dr Lee-Wei Yang (National Tsing Hua University, Hsinchu, Taiwan) for providing high-performance computing for MD simulations. We also thank the TechComm of National Taiwan University College of Life Science for supplying the core facilities for our use. We would like to thank Uni-edit (www.uni-edit.net) for editing and proofreading this manuscript.

FUNDING

Ministry of Science and Technology [106-2311-B-002-012-MY2, 107-2313-B-002-006]. Funding for open access charge: Ministry of Science and Technology.

Conflict of interest statement. None declared.

REFERENCES

1. Schroeder,R., Barta,A. and Semrad,K. (2004) Strategies for RNA folding and assembly. *Nat. Rev. Mol. Cell Biol.*, **5**, 908–919.
2. Mandal,M. and Breaker,R.R. (2004) Gene regulation by riboswitches. *Nat. Rev. Mol. Cell Biol.*, **5**, 451–463.
3. Schultes,E.A. and Bartel,D.P. (2000) One sequence, two ribozymes: implications for the emergence of new ribozyme folds. *Science*, **289**, 448–452.
4. Pan,T. and Sosnick,T. (2006) RNA folding during transcription. *Annu. Rev. Biophys. Biomol. Struct.*, **35**, 161–175.
5. Kramer,F.R. and Mills,D.R. (1981) Secondary structure formation during RNA synthesis. *Nucleic Acids Res.*, **9**, 5109–5124.
6. Uhm,H., Kang,W., Ha,K.S., Kang,C. and Hohng,S. (2018) Single-molecule FRET studies on the cotranscriptional folding of a thiamine pyrophosphate riboswitch. *Proc. Natl. Acad. Sci. U.S.A.*, **115**, 331–336.
7. Frieda,K.L. and Block,S.M. (2012) Direct observation of cotranscriptional folding in an adenine riboswitch. *Science*, **338**, 397–400.
8. Herschlag,D. (1995) RNA chaperones and the RNA folding problem. *J. Biol. Chem.*, **270**, 20871–20874.
9. Brion,P. and Westhof,E. (1997) Hierarchy and dynamics of RNA folding. *Annu. Rev. Biophys. Biomol. Struct.*, **26**, 113–137.
10. Treiber,D.K. and Williamson,J.R. (1999) Exposing the kinetic traps in RNA folding. *Curr. Opin. Struct. Biol.*, **9**, 339–345.
11. Doetsch,M., Schroeder,R. and Furtig,B. (2011) Transient RNA-protein interactions in RNA folding. *FEBS J.*, **278**, 1634–1642.
12. Woodson,S.A., Panja,S. and Santiago-Frangos,A. (2018) Proteins that chaperone RNA regulation. *Microbiol. Spectr.*, **6**, RWR-0026–2018.
13. Farabaugh,P.J. (1996) Programmed translational frameshifting. *Microbiol. Rev.*, **60**, 103–134.
14. Brierley,I., Gilbert,R.J.C. and Pennell,S. (2010) In: Atkins,J.F. and Gesteland,R.F. (eds). *Recoding: Expansion of Decoding Rules Enriches Gene Expression*. Springer, NY, Vol. **24**, pp. 149–174.
15. Dinman,J.D. (2012) Mechanisms and implications of programmed translational frameshifting. *Wiley Interdiscip. Rev.-RNA*, **3**, 661–673.
16. Atkins,J.F., Loughran,G., Bhatt,P.R., Firth,A.E. and Baranov,P.V. (2016) Ribosomal frameshifting and transcriptional slippage: From genetic steganography and cryptography to adventitious use. *Nucleic Acids Res.*, **44**, 7007–7078.
17. Korniy,N., Samatova,E., Anokhina,M.M., Peske,F. and Rodnina,M.V. (2019) Mechanisms and biomedical implications of -1 programmed ribosome frameshifting on viral and bacterial mRNAs. *FEBS Lett.*, **593**, 1468–1482.
18. Larsen,B., Gesteland,R.F. and Atkins,J.F. (1997) Structural probing and mutagenic analysis of the stem-loop required for *Escherichia coli dnaX* ribosomal frameshifting: programmed efficiency of 50%. *J. Mol. Biol.*, **271**, 47–60.
19. Bidou,L., Stahl,G., Grima,B., Liu,H., Cassan,M. and Rousset,J.P. (1997) In vivo HIV-1 frameshifting efficiency is directly related to the stability of the stem-loop stimulatory signal. *RNA*, **3**, 1153–1158.
20. Mouzakis,K.D., Lang,A.L., Vander Meulen,K.A., Easterday,P.D. and Butcher,S.E. (2013) HIV-1 frameshift efficiency is primarily determined by the stability of base pairs positioned at the mRNA entrance channel of the ribosome. *Nucleic Acids Res.*, **41**, 1901–1913.
21. Hansen,T.M., Reihani,S.N., Oddershede,L.B. and Sorensen,M.A. (2007) Correlation between mechanical strength of messenger RNA pseudoknots and ribosomal frameshifting. *Proc. Natl. Acad. Sci. U.S.A.*, **104**, 5830–5835.
22. Chen,G., Chang,K.Y., Chou,M.Y., Bustamante,C. and Tinoco,I. Jr (2009) Triplex structures in an RNA pseudoknot enhance mechanical stability and increase efficiency of -1 ribosomal frameshifting. *Proc. Natl. Acad. Sci. U.S.A.*, **106**, 12706–12711.
23. Ritchie,D.B., Foster,D.A. and Woodside,M.T. (2012) Programmed -1 frameshifting efficiency correlates with RNA pseudoknot conformational plasticity, not resistance to mechanical unfolding. *Proc. Natl. Acad. Sci. U.S.A.*, **109**, 16167–16172.
24. de Messieres,M., Chang,J.C., Belew,A.T., Meskauskas,A., Dinman,J.D. and La Porta,A. (2014) Single-molecule measurements of the CCR5 mRNA unfolding pathways. *Biophys. J.*, **106**, 244–252.
25. Ritchie,D.B., Soong,J., Sikkema,W.K. and Woodside,M.T. (2014) Anti-frameshifting ligand reduces the conformational plasticity of the SARS virus pseudoknot. *J. Am. Chem. Soc.*, **136**, 2196–2199.
26. Kuhlmann,M.M., Chattopadhyay,M., Stupina,V.A., Gao,F. and Simon,A.E. (2016) An RNA element that facilitates programmed ribosomal readthrough in turnip crinkle virus adopts multiple conformations. *J. Virol.*, **90**, 8575–8591.
27. Moomau,C., Musalgaonkar,S., Khan,Y.A., Jones,J.E. and Dinman,J.D. (2016) Structural and functional characterization of programmed ribosomal frameshift signals in West Nile Virus strains reveals high structural plasticity among *cis*-acting RNA elements. *J. Biol. Chem.*, **291**, 15788–15795.
28. Ritchie,D.B., Cappellano,T.R., Tittle,C., Rezajooei,N., Rouleau,L., Sikkema,W.K.A. and Woodside,M.T. (2017) Conformational dynamics of the frameshift stimulatory structure in HIV-1. *RNA*, **23**, 1376–1384.
29. Wu,B., Zhang,H., Sun,R., Peng,S., Cooperman,B.S., Goldman,Y.E. and Chen,C. (2018) Translocation kinetics and structural dynamics of ribosomes are modulated by the conformational plasticity of downstream pseudoknots. *Nucleic Acids Res.*, **46**, 9736–9748.
30. Halma,M.T.J., Ritchie,D.B., Cappellano,T.R., Neupane,K. and Woodside,M.T. (2019) Complex dynamics under tension in a high-efficiency frameshift stimulatory structure. *Proc. Natl. Acad. Sci. U.S.A.*, **116**, 19500–19505.
31. Halma,M.T.J., Ritchie,D.B. and Woodside,M.T. (2021) Conformational Shannon entropy of mRNA structures from force spectroscopy measurements predicts the efficiency of -1 programmed ribosomal frameshift stimulation. *Phys. Rev. Lett.*, **126**, 038102.
32. Plant,E.P. and Dinman,J.D. (2005) Torsional restraint: a new twist on frameshifting pseudoknots. *Nucleic Acids Res.*, **33**, 1825–1833.
33. Plant,E.P., Jacobs,K.L., Harger,J.W., Meskauskas,A., Jacobs,J.L., Baxter,J.L., Petrov,A.N. and Dinman,J.D. (2003) The 9-Å solution: how mRNA pseudoknots promote efficient programmed -1 ribosomal frameshifting. *RNA*, **9**, 168–174.
34. Namy,O., Moran,S.J., Stuart,D.I., Gilbert,R.J. and Brierley,I. (2006) A mechanical explanation of RNA pseudoknot function in programmed ribosomal frameshifting. *Nature*, **441**, 244–247.
35. Chang,K.C., Salawu,E.O., Chang,Y.Y., Wen,J.D. and Yang,L.W. (2019) Resolution-exchanged structural modeling and simulations jointly unravel that subunit rolling underlies the mechanism of programmed ribosomal frameshifting. *Bioinformatics*, **35**, 945–952.
36. Liu,T., Kaplan,A., Alexander,L., Yan,S., Wen,J.D., Lancaster,L., Wickersham,C.E., Fredrick,K., Noller,H., Tinoco,I. Jr *et al.* (2014) Direct measurement of the mechanical work during translocation by the ribosome. *eLife*, **3**, e03406.
37. Chen,J., Petrov,A., Johansson,M., Tsai,A., O'Leary,S.E. and Puglisi,J.D. (2014) Dynamic pathways of -1 translational frameshifting. *Nature*, **512**, 328–332.
38. Theimer,C.A., Blois,C.A. and Feigon,J. (2005) Structure of the human telomerase RNA pseudoknot reveals conserved tertiary interactions essential for function. *Mol. Cell*, **17**, 671–682.
39. Chou,M.Y. and Chang,K.Y. (2010) An intermolecular RNA triplex provides insight into structural determinants for the pseudoknot stimulator of -1 ribosomal frameshifting. *Nucleic Acids Res.*, **38**, 1676–1685.
40. Chen,Y.T., Chang,K.C., Hu,H.T., Chen,Y.L., Lin,Y.H., Hsu,C.F., Chang,C.F., Chang,K.Y. and Wen,J.D. (2017) Coordination among tertiary base pairs results in an efficient frameshift-stimulating RNA pseudoknot. *Nucleic Acids Res.*, **45**, 6011–6022.
41. Moffitt,J.R., Chemla,Y.R., Smith,S.B. and Bustamante,C. (2008) Recent advances in optical tweezers. *Annu. Rev. Biochem.*, **77**, 205–228.
42. Ritchie,D.B. and Woodside,M.T. (2015) Probing the structural dynamics of proteins and nucleic acids with optical tweezers. *Curr. Opin. Struct. Biol.*, **34**, 43–51.
43. Wen,J.D., Lancaster,L., Hodges,C., Zeri,A.C., Yoshimura,S.H., Noller,H.F., Bustamante,C. and Tinoco,I. Jr (2008) Following translation by single ribosomes one codon at a time. *Nature*, **452**, 598–603.
44. Wen,J.D., Manosas,M., Li,P.T., Smith,S.B., Bustamante,C., Ritort,F. and Tinoco,I. Jr (2007) Force unfolding kinetics of RNA using optical tweezers. I. Effects of experimental variables on measured results. *Biophys. J.*, **92**, 2996–3009.

45. Smith,S.B., Cui,Y. and Bustamante,C. (2003) Optical-trap force transducer that operates by direct measurement of light momentum. *Methods Enzymol.*, **361**, 134–162.
46. Li,P.T., Collin,D., Smith,S.B., Bustamante,C. and Tinoco,I. Jr (2006) Probing the mechanical folding kinetics of TAR RNA by hopping, force-jump, and force-ramp methods. *Biophys. J.*, **90**, 250–260.
47. Li,P.T., Vieregg,J. and Tinoco,I. Jr (2008) How RNA unfolds and refolds. *Annu. Rev. Biochem.*, **77**, 77–100.
48. Melkonyan,L., Bercy,M., Bizebard,T. and Bockelmann,U. (2019) Overstretching double-stranded RNA, double-stranded DNA, and RNA-DNA duplexes. *Biophys. J.*, **117**, 509–519.
49. Bustamante,C., Marko,J.F., Siggia,E.D. and Smith,S. (1994) Entropic elasticity of lambda-phage DNA. *Science*, **265**, 1599–1600.
50. Wang,M.D., Yin,H., Landick,R., Gelles,J. and Block,S.M. (1997) Stretching DNA with optical tweezers. *Biophys. J.*, **72**, 1335–1346.
51. Liphardt,J., Onoa,B., Smith,S.B., Tinoco,I. Jr and Bustamante,C. (2001) Reversible unfolding of single RNA molecules by mechanical force. *Science*, **292**, 733–737.
52. Yang,L., Zhong,Z., Tong,C., Jia,H., Liu,Y. and Chen,G. (2018) Single-molecule mechanical folding and unfolding of RNA hairpins: effects of single A-U to A·C pair substitutions and single proton binding and implications for mRNA structure-induced -1 ribosomal frameshifting. *J. Am. Chem. Soc.*, **140**, 8172–8184.
53. Schurer,H., Lang,K., Schuster,J. and Morl,M. (2002) A universal method to produce in vitro transcripts with homogeneous 3′ ends. *Nucleic Acids Res.*, **30**, e56.
54. Liu,D., Shao,Y., Chen,G., Tse-Dinh,Y.C., Piccirilli,J.A. and Weizmann,Y. (2017) Synthesizing topological structures containing RNA. *Nat. Commun.*, **8**, 14936.
55. Stone,M.D., Mihalusova,M., O'Connor,C.M., Prathapam,R., Collins,K. and Zhuang,X. (2007) Stepwise protein-mediated RNA folding directs assembly of telomerase ribonucleoprotein. *Nature*, **446**, 458–461.
56. Lee,H.W., Ryu,J.Y., Yoo,J., Choi,B., Kim,K. and Yoon,T.Y. (2013) Real-time single-molecule coimmunoprecipitation of weak protein-protein interactions. *Nat. Protoc.*, **8**, 2045–2060.
57. Roy,R., Hohng,S. and Ha,T. (2008) A practical guide to single-molecule FRET. *Nat. Methods*, **5**, 507–516.
58. Rother,M., Rother,K., Puton,T. and Bujnicki,J.M. (2011) ModeRNA: a tool for comparative modeling of RNA 3D structure. *Nucleic Acids Res.*, **39**, 4007–4022.
59. Theimer,C.A., Finger,L.D., Trantirek,L. and Feigon,J. (2003) Mutations linked to dyskeratosis congenita cause changes in the structural equilibrium in telomerase RNA. *Proc. Natl. Acad. Sci. U.S.A.*, **100**, 449–454.
60. Zhong,Z., Soh,L.H., Lim,M.H. and Chen,G. (2015) A U·U pair-to-U·C pair mutation-induced RNA native structure destabilisation and stretching-force-induced RNA misfolding. *ChemPlusChem*, **80**, 1267–1278.
61. Wu,Y.J., Wu,C.H., Yeh,A.Y. and Wen,J.D. (2014) Folding a stable RNA pseudoknot through rearrangement of two hairpin structures. *Nucleic Acids Res.*, **42**, 4505–4515.
62. Qu,X., Wen,J.D., Lancaster,L., Noller,H.F., Bustamante,C. and Tinoco,I. Jr (2011) The ribosome uses two active mechanisms to unwind messenger RNA during translation. *Nature*, **475**, 118–121.
63. Yusupova,G.Z., Yusupov,M.M., Cate,J.H. and Noller,H.F. (2001) The path of messenger RNA through the ribosome. *Cell*, **106**, 233–241.
64. Amiri,H. and Noller,H.F. (2019) A tandem active site model for the ribosomal helicase. *FEBS Lett.*, **593**, 1009–1019.
65. Amiri,H. and Noller,H.F. (2019) Structural evidence for product stabilization by the ribosomal mRNA helicase. *RNA*, **25**, 364–375.
66. Roca,J., Hori,N., Baral,S., Velmurugu,Y., Narayanan,R., Narayanan,P., Thirumalai,D. and Ansari,A. (2018) Monovalent ions modulate the flux through multiple folding pathways of an RNA pseudoknot. *Proc. Natl. Acad. Sci. USA*, **115**, E7313–E7322.
67. Cho,S.S., Pincus,D.L. and Thirumalai,D. (2009) Assembly mechanisms of RNA pseudoknots are determined by the stabilities of constituent secondary structures. *Proc. Natl. Acad. Sci. U.S.A.*, **106**, 17349–17354.
68. Smith,A.M., Costello,M.S., Kettring,A.H., Wingo,R.J. and Moore,S.D. (2019) Ribosome collisions alter frameshifting at translational reprogramming motifs in bacterial mRNAs. *Proc. Natl. Acad. Sci. U.S.A.*, **116**, 21769–21779.
69. Plant,E.P., Perez-Alvarado,G.C., Jacobs,J.L., Mukhopadhyay,B., Hennig,M. and Dinman,J.D. (2005) A three-stemmed mRNA pseudoknot in the SARS coronavirus frameshift signal. *PLoS. Biol.*, **3**, e172.
70. Su,M.C., Chang,C.T., Chu,C.H., Tsai,C.H. and Chang,K.Y. (2005) An atypical RNA pseudoknot stimulator and an upstream attenuation signal for -1 ribosomal frameshifting of SARS coronavirus. *Nucleic Acids Res.*, **33**, 4265–4275.
71. Chen,X., Chamorro,M., Lee,S.I., Shen,L.X., Hines,J.V., Tinoco,I. Jr and Varmus,H.E. (1995) Structural and functional studies of retroviral RNA pseudoknots involved in ribosomal frameshifting: nucleotides at the junction of the two stems are important for efficient ribosomal frameshifting. *EMBO J.*, **14**, 842–852.
72. Shen,L.X. and Tinoco,I. Jr (1995) The structure of an RNA pseudoknot that causes efficient frameshifting in mouse mammary tumor virus. *J. Mol. Biol.*, **247**, 963–978.
73. Kang,H., Hines,J.V. and Tinoco,I. Jr (1996) Conformation of a non-frameshifting RNA pseudoknot from mouse mammary tumor virus. *J. Mol. Biol.*, **259**, 135–147.
74. Semrad,K. and Schroeder,R. (1998) A ribosomal function is necessary for efficient splicing of the T4 phage thymidylate synthase intron in vivo. *Genes Dev.*, **12**, 1327–1337.
75. Pichler,A. and Schroeder,R. (2002) Folding problems of the 5′ splice site containing the P1 stem of the group I thymidylate synthase intron: substrate binding inhibition in vitro and mis-splicing in vivo. *J. Biol. Chem.*, **277**, 17987–17993.
76. Clodi,E., Semrad,K. and Schroeder,R. (1999) Assaying RNA chaperone activity in vivo using a novel RNA folding trap. *EMBO J.*, **18**, 3776–3782.